RSC Advances

This is an *Accepted Manuscript*, which has been through the Royal Society of Chemistry peer review process and has been accepted for publication.

Accepted Manuscripts are published online shortly after acceptance, before technical editing, formatting and proof reading. Using this free service, authors can make their results available to the community, in citable form, before we publish the edited article. This *Accepted Manuscript* will be replaced by the edited, formatted and paginated article as soon as this is available.

You can find more information about *Accepted Manuscripts* in the Information for Authors.

Please note that technical editing may introduce minor changes to the text and/or graphics, which may alter content. The journal's standard Terms & Conditions and the Ethical guidelines still apply. In no event shall the Royal Society of Chemistry be held responsible for any errors or omissions in this *Accepted Manuscript* or any consequences arising from the use of any information it contains.

ROYAL SOCIETY OF CHEMISTRY

www.rsc.org/advances

Eco-friendly water-induced aluminum oxide dielectrics and their applications in hybrid metal oxide/polymer TFT

Ao Liu,[a] Guoxia Liu,[aξ] Huihui Zhu,[a] Byoungchul Shin,[b] Elvira Fortunato,[c] Rodrigo Martins[c], and Fukai Shan[a*]

[a]*College of Physics and Lab of New Fiber Materials and Modern Textile, Growing Base for State Key Laboratory, Qingdao University, Qingdao 266071, China*

[b]*Electronic Ceramics Center, DongEui University, Busan 614-714, Korea*

[c]*Department of Materials Science/CENIMAT-I3N, Faculty of Sciences and Technology, New University of Lisbon and CEMOP-UNINOVA, Campus de Caparica, 2829-516 Caparica, Portugal*

Abstract: Solution-processed oxide semiconductors have been widely studied with the objective of achieving high-performance, sustainable and low-cost electronic devices. In this report a simple and eco-friendly water-inducement method has been developed to fabricate high-*k* dielectrics and hybrid thin-film transistors (TFTs); introducing metal nitrates and deionized water as the precursor materials. The AlO_x dielectrics films annealed at temperatures higher than 350 °C result in low leakage current densities and the dielectric constants are nearly 7. Instead of the conventional oxide semiconductors, water-induced (WI) polyvinylprrolidone (PVP) was introduced into In_2O_3 solution to form a hybrid metal oxide/polymer channel layer. The 250 °C-annealed WI In_2O_3:PVP TFTs based on AlO_x dielectric exhibit outstanding electrical performances and high stability. These promising properties were obtained at an ultra-low operating voltage of 2 V. The WI metal oxide/polymer hybrid TFTs are promising alternatives for the applications in low-cost, low-consumption and eco-friendly flexible electronics.

ξ Correspondence should be addressed: gxliu@qdu.edu.cn
* Corresponding author: fukaishan@yahoo.com

RSC Advances Accepted Manuscript

1. Introduction

As potential alternatives for thin-film transistors (TFTs) based on conventional silicon technologies, amorphous metal-oxide TFTs are of great interest due to the high carrier mobility, high transparency, excellent large-area uniformity, and solution processability.[1-4] Recently, the electronic devices fabricated via solution process have been regarded as a key part of next-generation processing technique. To achieve oxide TFTs at low temperatures, several research groups proposed novel annealing approaches, such as sol-gel on chip,[5] self-combustion process through an oxidizer and fuel,[6] and photochemical activation method.[7] However, in these reports, all the precursor solutions were synthesized using organic solvents, e.g. 2-methoxyethanol (2-ME) and methoxyisopropanol, which is toxic to humans and harmful to the environment. Additional additives or follow-up processing steps also increase the environment damage and the fabrication cost. Meanwhile, it is noted that most of these novel approaches are focused on the achievement of channel layers, which restrict the development of low-cost solution-processed TFTs at low temperature. Most recently, Bae *et al.* adopted 'self-combustion' method to prepare the high-*k* AlO_x dielectric and the oxide TFTs were integrated successfully.[8] However, the small on/off current ratio ($\sim 10^5$) and large operation voltage (> 20 V) can not meet the requirements of low-consumption active-matrix TFTs.

The use of appropriate metal precursors, solvents, and gate dielectrics is crucial to enable low-temperature processing and high device performance.[9] In order to achieve high-performance solution-processed oxide TFTs at low temperature, all these aspects should be taken into account. The nitrate salts, which are low cost and readily available, have been proved to require less thermal energy to be decomposed completely compared with other salts, e.g. acetates, and chlorides.[10, 11] Meanwhile, as a solvent, water meets the current environmental awareness restricting the use of ecologically harmful substances and process. Instead of the often used organic-based solvents, the water-inducement route is considered to be simpler, safer and environmentally friendlier.[12-14] As environment protection is an important issue, the use of nontoxic materials and employment of eco-friendly processes in the industry is strongly required. One more important issue is that the TFT device based on high-*k* dielectric can be operated at relatively low voltage and hence less power will be consumed. Among various high-*k* dielectrics, AlO_x has been studied most extensively

RSC Advances Accepted Manuscript

because of its high conduction band offset,[15] low interface trap density,[16] and its high chemical stability.[17] The water-induced (WI) AlO_x dielectric thin film could be an ideal candidate for the application in low-cost, eco-friendly and low-consumption electronic devices.

To achieve acceptable TFT performance, a channel layer with high mobility and low carrier concentration is also required. Generally, strong oxygen-binding cations, e.g., X = Y,[18] Ga,[11, 19] Ti,[20] and Al,[21] are introduced into In_2O_3 host as matrix dopants to adjust the carrier concentration. Meanwhile, the mixture of various metal oxides will lead to the uniform amorphous nature and smooth surface due to the absence of the grain boundaries. However, for the TFTs based on solution-processed IXO channel layer, relatively high processing temperature (typically $\geq$ 300 ^oC) is usually necessary to facilitate the impurity removal, densification, and the alloy formation. This is incompatible with plastic substrates. The organic/inorganic hybrid material represents a major advance because of its flexibility and the low temperature characteristic.[22, 23] Meanwhile, in the previous reports, the toxic organic solvents and the complicated preparation process were usually involved. This undoubtedly limits the application in the future solution-based electronics.

By using water-inducement synthetic method, we employed a simple, sustainable and eco-friendly process to fabricate the high-*k* AlO_x dielectric and the WI hybrid TFTs. The annealing effects on the properties of WI AlO_x thin films and the storage stability of precursor solution were investigated. The optimized WI metal oxide/polymer hybrid channel layer can be achieved by doping PVP into In_2O_3 and processed at temperature as low as 250 ^oC. By excluding hazardous organic solvents, the 'green' process will certainly contribute to environmental safety and cost minimization simultaneously.

2. Experiment section

2.1 Precursor Solution Preparations and Characterization.

The WI AlO_x precursor solution with concentration of 0.1 M was prepared by dissolving aluminum nitrate nonahydrate ($Al(NO_3)_3•9H_2O$) in de-ionized (DI) water. For comparison, AlO_x precursor solution with 2-methoxyethanol as solvent at the same concentration was prepared. The hybrid In_2O_3 and PVP mixed precursor solution was prepared by adding WI PVP ($M_w \approx 25000$ g mL^{-1}) solution into WI In_2O_3 precursor solution with a PVP weight fraction of 5%.[23] All precursor solutions

RSC Advances Accepted Manuscript

were stirred vigorously for 6 h under ambient conditions before spin coating. The thermal behaviors of the AlO_x xerogel based on different solvents and the WI PVP xerogel were monitored under air ambient by using a thermal-gravimetric analyzer (TGA, Pyris1) with heating rate of 10 ^oC/min. To clarify the storage stability of WI AlO_x precursor solution, the solution was aged for 3, 15, and 30 days, respectively. The solution was magnetically stirred for 15 min before spin coating.

2.2 Thin Film Fabrication and Characterization.

Heavily doped p-type silicon wafers with resistivity of 0.001 Ω cm were used as gate electrode and substrate. Prior to thin film fabrication, all substrates were cleaned ultrasonically in 2 % HF acid, acetone, ethanol, and DI water in sequence and dried by N_2 gun. The substrates were then exposed under oxygen plasma for 5 min to enhance the hydrophilicity. The WI AlO_x precursor solution was spun on the substrates at 5000 rpm for 20 s and baked at 150 ^oC for 10 min. This procedure was repeated twice to obtain an appropriate thickness. After that, the samples were post-annealed by a sequential process including a UV-assisted treatment for 40 min and thermal annealing process in the temperature range from 150 to 450 ^oC for 2 h in air. The UV lamp power was 1 kW with the peak at 365 nm and abroad bands between 200 nm and 320 nm. The distance from the sample to the UV lamp was 10 cm. For convenience, the AlO_x thin films annealed at 150, 250, 350, and 450 ^oC, hereafter, will be abbreviated as AlO_x-150, AlO_x-250, AlO_x-350, and AlO_x-450, respectively.

The crystal structures of AlO_x thin films were investigated by X-ray diffractometer (XRD, X'Pert-PRO MPD and MRD, PANalytical, Holland) with a Cu*K*α1 radiation. The surface morphologies of AlO_x thin films were measured by using an atomic force microscope (AFM, SPA-400, Seiko). The chemical compositions of AlO_x thin films were analyzed by X-ray photoelectron spectroscopy (XPS, ESCALAB 250). The chemical bonding characteristics of the AlO_x thin films were measured by Fourier transform infrared (FT-IR, Nicolet 5700). The thicknesses of AlO_x thin films were measured by ellipsometry (ESS01, Sofn Instrument).

2.3 Electronic Device Fabrication and Characteristics.

The capacitors with a structure of Al/AlO_x/p^+-Si were fabricated to evaluate the dielectric properties of the AlO_x thin films annealed at various temperatures. The dielectric properties of the thin films were investigated by an impedance analyzer (Agilent 4294A). To fabricate the hybridized TFT devices based on the AlO_x

RSC Advances Accepted Manuscript

dielectrics, the In_2O_3:PVP precursor solution was spun on AlO_x-350 at 4500 rpm for 20 s. The laminated thin films were subsequently annealed at various temperatures (from 230 to 300 °C) for 1 h. Finally, Al source and drain electrodes were deposited on In_2O_3:PVP channel layer by thermal evaporation through a shadow mask. In this report, the channel length and width of the TFTs were 250 and 1000 μm, respectively. The electrical properties of AlO_x capacitors and the TFT devices were investigated by using a semiconductor parameter analyzer (Keithley 2634B) in a dark box. The saturation mobility (μ_{sat}) was extracted from transfer characteristics using the following equation[24]

$$I_{DS} = \left(\frac{W}{2L} C_i \mu_{sat}\right) (V_G - V_{TH})^2 \quad (1)$$

where C_i is the areal capacitance of the gate dielectric , W and L are the channel width and length of the TFT, V_G is the gate voltage and V_{TH} is the threshold voltage, which was determined in the saturation region by linear fitting $I_D^{1/2}$ vs V_G plot. The maximum areal density of states (N_s^{max}) at semiconductor/dielectric interface of the TFT device was calculated using the following equation[25]

$$N_s^{max} = \left[\frac{SS \times \log e}{kT/q} - 1\right] \frac{C_i}{q} \quad (2)$$

where k is the Boltzmann constant, q is the electron charge, e is the base of natural logarithm, SS is subthreshold swing of the transfer curve.

3. Results and discussion

The combination of metal nitrates and water as the precursors and solvent provides a simple and unique structure in a solution state. Water is a frequently-used solvent with a high static dielectric constant of ~80 at room temperature, which favors the dissociation of ionic species and acts as the σ-donor molecule that reacts as a nucleophilic ligand. When the metal nitrates were dissolved in water, the ionized metal cation, M^{n+}, is solvated by the neighboring water molecules. The number of solvating water molecules and the bond type depend basically on the polarizing strength (Z/r^2) of the metal ion, where Z is effective nuclear charge and r is ionic radius.[26] So, the small-size and high-charge cations have strong electrostatic interactions with water molecules, which are beneficial to form stable precursor solution. Among these frequently-used metal elements, Al was found to have the largest polarizing strength, 6.58, as shown in Fig. 1.[27] Therefore, compared with other

RSC Advances Accepted Manuscript

WI high-*k* binary oxide materials, AlO_x will be a promising candidate due to its high precursor stability.

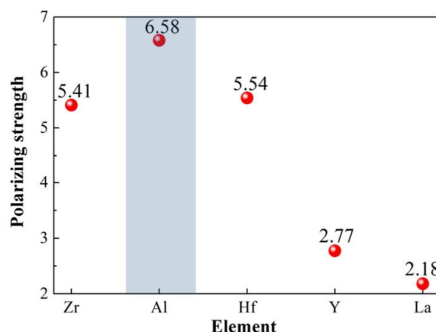

Fig.1 Polarizing strength of various high-*k* metal elements.

The thermogravimetric analysis of the precursor solutions, shown in Fig. 2, indicates that the thermal decomposition temperature was substantially decreased in the WI AlO_x solution. The decomposition temperature of the WI AlO_x solution was completed at ~350 °C, whereas the decomposition temperature for the 2-ME-based AlO_x solution was approximately 500 °C. The low-temperature decomposition behavior of the WI solution is strongly related to the unique structure of aluminum complex. As the coordination bond between the Al^{3+} and neighboring aquo ion is electrostatic reaction, it is easily broken with small thermal energy compared to the covalent bond in the conventional organic-based precursor.[12, 13]

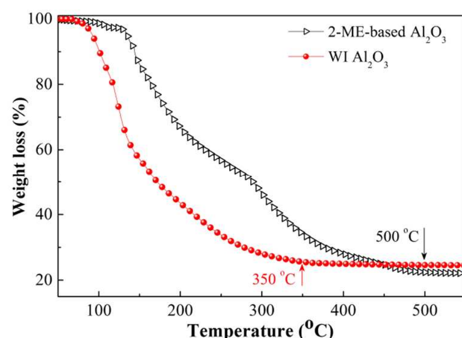

Fig. 2 Thermal behaviors of the WI and 2-ME-based AlO_x xerogel. The WI solution and 2-ME-based solution are denoted by the red (solid circle) and black (open triangle) lines, respectively.

Based on the low-temperature decomposition characteristic of the WI AlO_x precursor solution, the structural properties of the corresponding AlO_x thin films annealed at various temperatures (from 150 °C to 450 °C) were examined, and are shown in Fig. S1 (ESI). No peak corresponding to the crystalline AlO_x was observed, suggesting amorphous AlO_x films were obtained over the entire annealing

RSC Advances Accepted Manuscript

temperature range. This is consistent with the previous report that the AlO_x thin film was crystallized at temperature up to 1000 °C.[28] The amorphous state has advantages over the crystalline phase because the grain boundaries might act as diffusion paths, cause large leakage current, and fluctuate the *k* value from grain to grain.

Generally, a desirable criterion for the solution-processed insulating materials applying as gate dielectrics in TFTs is that the surface roughness should be as small as possible. In this work, the root mean square (RMS) surface roughness of the WI AlO_x-150, AlO_x-250, AlO_x-350, and AlO_x-450 with UV-assisted pretreatment were 0.35, 0.29, 0.40, and 0.33 nm, respectively. The corresponding surface morphologies of AlO_x thin films were shown in Fig. S2 (ESI). The smooth surfaces of the AlO_x thin films are undoubtedly beneficial from the organic-species-free precursor solution. Little volatile gas overflowed from WI thin film surface during pyrolysis process, so the thin film surface can be kept as smooth as possible. Meanwhile, it is found that the surface morphologies of AlO_x thin films were improved with a UV-assisted pretreatment than that of the thermally-annealed samples without UV treatment, as shown in Fig. 3(a). To clarify the possible reaction occurred during UV treatment, the UV-visible absorption spectrum of the precursor solution was investigated and the result is shown in Fig. 3(b). The WI solution exhibits light absorption below the wavelength of 350 nm. This is expected, as the absorption originates from the nitrate anion.[29] The nitrate anion will be readily decomposed under UV exposure, as described by equations (3)-(5). It is suggested that excitation in the π*←π band (λ < 280 nm) proceeds via the two primary photon processes (3) and (4), whereas excitation in the π*←n band (λ > 280 nm) proceeds through steps (3) and (5).[30, 31]

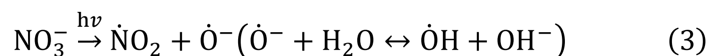

$$NO_3^- \xrightarrow{h\upsilon} \dot{N}O_2 + \dot{O}^- \left(\dot{O}^- + H_2O \leftrightarrow \dot{O}H + OH^-\right) \tag{3}$$

$$\xrightarrow{h\upsilon} ONOO^- \tag{4}$$

$$\xrightarrow{h\upsilon} NO_2^- + \dot{O} \tag{5}$$

Although the UV decomposition mechanisms of the nitrate anion are complex, oxygen and nitrogen dioxide radicals are surely formed during UV irradiation. This combinative process improves the interface properties, which is important for TFT applications in terms of device performance and stability because the charge carriers always move along the interface between the semiconductor and the gate dielectric.

RSC Advances Accepted Manuscript

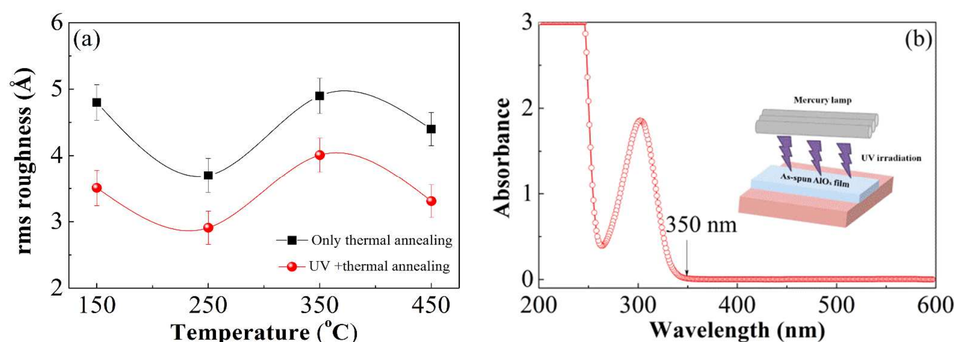

Fig. 3 (a) The RMS values of WI AlO_x thin films prepared at various conditions. (b) The UV-visible absorption spectra of AlO_x precursor solution. The inset in (b) shows a schematic illustration of the UV irradiation from a mercury lamp.

The chemical composition of the WI AlO_x thin films was investigated by XPS measurements. All the XPS peaks are calibrated by taking C 1s reference at 284.8 eV to compensate any charge-induced shift. The O 1s binding energies of the AlO_x thin films fabricated at various temperatures are shown in Fig. 4(a). The binding energies of the O 1s peaks were divided into three peaks centered at 530.3 eV, 531.2 eV, and 532.3 eV, respectively. In addition to the oxygen atoms with a binding energy of 531.2 eV from the AlO_x matrix, the oxygen species with a higher binding energy of 532.3 eV can be assigned to the bonded oxygen such as oxygen vacancies or OH^- during film fabrication process.[32] The oxygen species with a lower binding energy of 530.3 eV may be attributed to AlO(OH) component generated during the hydrolysis.[33] For convenience, O_I, O_{II}, and O_{III} denote the area of each component, and O_{tot} denotes the total area of the O 1s peak. It is found that, with increasing annealing temperature from 150 to 450 °C, the fraction of bonded oxygen in AlO_x was decreased from 48.6% to 26.8%. This indicates that the oxidation of AlO_x thin films removes the bonded oxygen and creates metal-oxygen bonds. The amount of bonded oxygen in the dielectric thin films should be small enough because the bonded oxygen species provide defect states in the bandgap of AlO_x, which can increase the leakage current and lower the breakdown electric field.[34]

Fig. 4(b) shows the Al 2p peaks of the AlO_x films prepared at different annealing temperatures. The XPS spectra show a single Al 2p peak at 74.3 eV in case of AlO_x-150 °C, whereas, it was shifted to lower binding energy for the AlO_x films annealed at higher temperatures. The shift of the Al 2p peak towards lower binding energy at higher processing temperatures is mainly attributed to the decrease of the concentration of OH^- ions or coordination number of Al^{3+} ions in the film.[9] To

RSC Advances Accepted Manuscript

understand the pyrolysis behavior of nitrate groups in AlO_x thin films, the N 1s peaks via XPS measurement were investigated and are shown in Fig. 4(c). Three peaks centered at 400.0 eV, 403.7 eV, and 407.0 eV were observed in AlO_x-150, which were assigned to nitrogen located in the interstitial sites, NO_2, and NO_3-related groups, respectively.[35] When the annealing temperature was increased to 350 °C, the nitrogen-related groups were undetectable. The similar pyrolysis behaviors of nitrate groups were also observed in the FT-IR spectra (Fig. S3, ESI). This indicates that the progressive oxidation of AlO_x thin film with pyrolysis of nitrogen-related groups occurred during thermal annealing process.

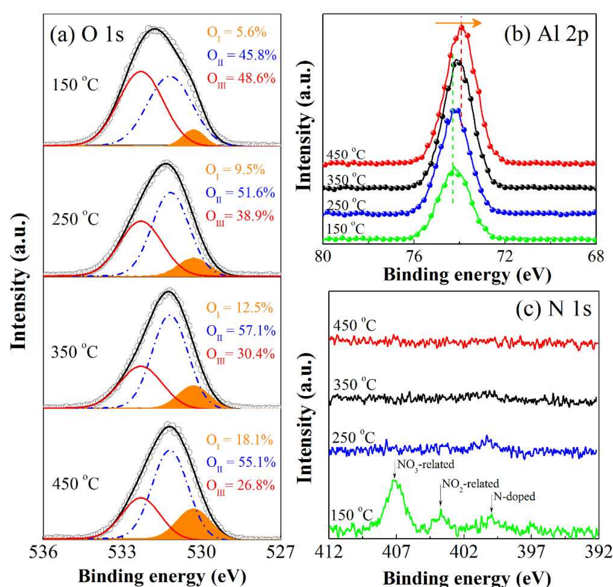

Fig. 4 (a) XPS spectra of O 1s peaks for AlO_x thin films annealed at different temperatures. XPS (b) Al 2p and (c) N 1s spectra of AlO_x thin films annealed at different temperatures.

Fig. 5(a) shows the areal capacitance (*C*) as a function of frequency (*f*) for AlO_x capacitors. The data show that the high frequency limit for which the capacitance almost saturates depends on the process temperature used, shifting from about 3 kHz for AlO_x-150 to about 70 kHz for AlO_x-450, where the capacitances exhibited are of about 400 nF/cm^2 and 450 nF/cm^2, respectively. The dielectric constants for AlO_x-150, AlO_x-250, AlO_x-350, and AlO_x-450 were taken from the capacitance flat region leading to values of around 6.95, 6.9, 7.0 and 7.1, respectively. (see Table S1, ESI). The permittivity values are somewhat smaller than the expected value for Al_2O_3, ~9, meaning that films are less dense and out of stoichiometry; These data are in agreement with reported values for solution-processed AlO_x.[17, 36] At low frequency

RSC Advances Accepted Manuscript

region, the areal capacitance decreases as the annealing temperature increases from 150 to 250 ^{o}C and then increases slightly for samples annealed at temperatures higher than 250 ^{o}C. We attribute the trends between 150 and 250 ^{o}C to the removal of nitrates, hydroxides, and absorbed water, reducing the amount of mobile charge species in the films. The presence of mobile charge species also contributes to the overall polarizability of the material. At temperatures above 250 ^{o}C, most of the mobile ions are removed, so the increase of the areal capacitance density can be attributed to the densification of the remaining metal-oxide framework.

The leakage current density (J_{leak})-electric field (E) measurements were performed to evaluate the leakage behavior of the corresponding AlO_x films, as shown in Fig. 5(b). It can be seen that the J_{leak} is high for AlO_x-150 (~10^{-5} A/cm^2 at 1 MV/cm), which is likely related to the defects associated with incomplete decomposition. The residual nitrate and hydroxyl groups provide a leakage current path, resulting in a high J_{leak}. The leakage current profiles were found to decrease in slope with increasing annealing temperature, suggesting a reduction in the electronic defects.[37] The current density levels for devices annealed at 350 ^{o}C and 450 ^{o}C were similar, less than 10^{-9} A/cm^2 at 1 MV/cm. The relative low J_{leak} and high breakdown field may originate from the smooth surface, relatively dense film, and high oxidation states with small numbers of hydroxyl groups in the films. Practically, annealing temperature lower than 350 ^{o}C is needed to employ solution process in conventional fabrication process of flat-panel displays.[38] Based on the electrical performances of WI AlO_x thin films annealed at different temperatures, AlO_x-350 undoubtedly meets the requirements as the gate dielectric for TFT device.

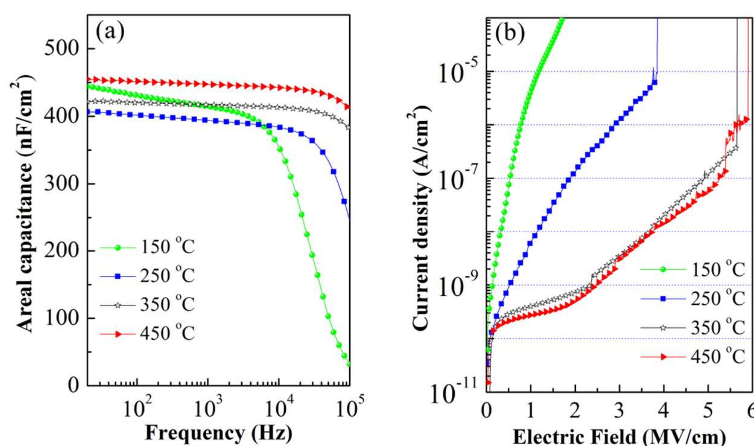

Fig. 5 Variation of the (a) C-f and (b) J_{leak}-E characteristics for $Al/AlO_x/p^+$-Si capacitors.

RSC Advances Accepted Manuscript

Most recently, Branquinho *et al.* proposed a novel 'combustion' method to synthesize AlO_x dielectrics using water as the solvent instead of the conventional 2-ME solvent.[17] The optimized AlO_x dielectrics and the integrated TFT devices exhibited high performance at a moderate annealing temperature of 350 ^{o}C. However, the aqueous combustion AlO_x precursor solution is unstable because the areal capacitance of the AlO_x capacitor decreased with increasing solution aging time. Practically, the storage stability of the precursor solution is an important issue in sol-gel chemistry. To clarify the storage stability of WI AlO_x precursor solution, the AlO_x capacitors fabricated by the precursor solution aged for different time intervals were compared. The *C-V* characteristics were investigated from -4 V to 0 V at 100 kHz. Three sequential loop measurements were carried out to investigate the reliability of AlO_x capacitors. Fig. 6 shows the *C-V* curves of AlO_x without solution aging. The capacitance value as a function of precursor aging time is summarized and shown in the inset of Fig. 6. The corresponding *C-V* curves of AlO_x capacitors with various aging time can be found in Fig. S4 (ESI). Interestingly, the AlO_x capacitors exhibited similar areal capacitances and negligible hysteresis over the entire range of aging time, which indicates high storage stability of WI AlO_x precursor solution. The high stability is not only beneficial from the large polarizing strength of Al (Fig. 1), but also the unique structure of WI precursor solution. The neighboring aquo ligand can effectively prevent the chemical reactions, hydrolysis and condensation.[13] Water-inducement synthesis is regarded as a promising chemical fabrication technique for future solution-based microelectronics.

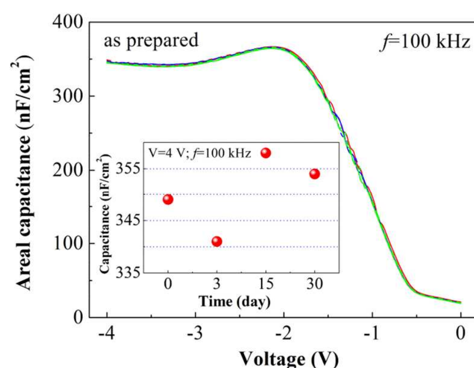

Fig. 6 *C-V* characteristics of $Al/AlO_x/p^+$-Si capacitors produced from the as-prepared precursor solution without aging treatment. The inset shows the summarized capacitance value as a function of precursor aging time.

In this work, PVP was chosen as the organic dopant for the hybrid channel layer because of its unique characteristics. PVP is highly soluble in polar solvents such as

RSC Advances Accepted Manuscript

water, it is preferable to avoid phase separation in the reaction.[39] Another advantage is that PVP can be thermally crosslinked, resulting in outstanding thermal stability and high mechanical strength of the hybrid material.[40] Furthermore, the amorphous nature of PVP also presents low electron scattering, which makes it an ideal polymer for hybrid channel layer materials. The thermal behavior of WI PVP xerogel was examined and found that the PVP was thermally stable until the annealing temperature reached 380 ^{o}C. It can be deduced that the PVP did not decompose during the annealing process for hybrid In_2O_3:PVP channel layers. For conventional metal oxide doping method, the larger M-O bonding strength than In-O bonding undoubtedly increases the post-processing temperature. However, in PVP doped In_2O_3 hybrid system, the required temperature has different meaning because PVP does not participate in the bond-forming reaction. The existence of insulating PVP can also effectively adjust the highly conductive property of pristine In_2O_3 matrix, which increases the reliability and stability of the fabricated TFT devices.

To investigate the performance of WI In_2O_3:PVP TFTs based on AlO_x-350 dielectric, TFT devices with bottom-gate and top-contact architecture were fabricated. The transfer characteristics of various In_2O_3:PVP TFTs with a double-sweep gate voltage model are shown in Fig. 7(a). It can be seen that the operating voltage of the TFT devices is only 2 V, which is important for low-power electronics. All of these TFTs show hysteresis characteristics, and their direction is clockwise. The presence of clockwise hysteresis indicates that accumulated electrons are trapped at/near the channel/dielectric interface or within the channel layer.[41] This hysteresis phenomenon is found to be improved with increasing annealing temperature. Since the same AlO_x dielectric thin films were used, the film qualities should be comparable, and the improvement in hysteresis phenomenon at higher annealing temperature should be attributed to the decreased amount of trap defects in channel layers. The corresponding electrical parameters of the In_2O_3:PVP TFTs annealed at various temperatures are summarized in Table 1.

RSC Advances Accepted Manuscript

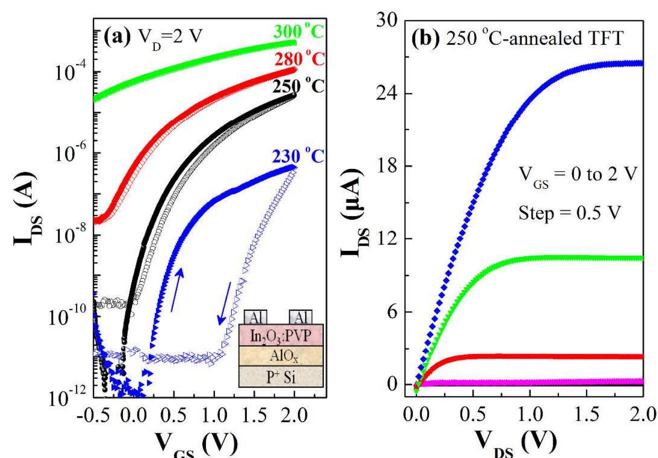

Fig. 7 (a) Transfer characteristics of In_2O_3:PVP TFTs at $V_D = 2$ V as a function of the annealing temperature. (b) The output curves of 250 °C-annealed In_2O_3:PVP TFT.

With the increase of the annealing temperature, the high on-state current (I_{on}) and large μ_{sat} were achieved; whereas the off-state current (I_{off}) was increased. The significant variation of the device performance in such a small temperature range is mainly attributed to the dehydroxylation and the alloy reaction in In_2O_3:PVP gel film (Fig. S5, ESI). It is known that the conduction band minimum in metal oxide semiconductors is primarily composed of dispersed vacant s states with short interaction distances for efficient carrier transportation, which can be achieved in ionic oxide but not obviously in hydroxide.[42] For this reason, the electron transportation property of the In_2O_3:PVP TFTs was improved at higher annealing temperatures. The more detailed explanation for the solution-processed oxide TFTs as a function of annealing temperature could be found in our previous report.[12]

Table 1. Electrical performance of In_2O_3:PVP TFTs as function of annealing temperature.

In_2O_3:PVP annealing temperature	μ_{sat} (cm^2/Vs)	I_{on}/I_{off}	V_{TH} (V)	SS (mV/dec)	Hysteresis (V)
230 °C	0.2±0.08	10^5-10^6	0.65±0.05	110±10	0.95±0.1
250 °C	14.1±0.5	~10^7	0.50±0.03	80±5	0.10±0.02
280 °C	22.5±0.6	10^3-10^4	0.18±0.02	310±20	0.07±0.01
300 °C	Conductive (TFT always on)				

It can be seen from Table 1 that the 250 °C-annealed In_2O_3:PVP/AlO_x TFT showed the best performance, including a μ_{sat} of 14.1 cm^2/Vs, a V_{TH} of 0.5 V, a turn-

RSC Advances Accepted Manuscript

on voltage (V_{on}) close to 0 V, and a high on/off current ratio (I_{on}/I_{off}) of 2×10^7. The output curves of 250 °C-annealed In_2O_3:PVP TFT is shown in Fig. 7(b). The device exhibits typical n-channel behavior with clear pinch-off and current saturation. Particularly, a small SS value, which is defined as the V_D required to increase the I_D by one decade, was calculated to be 80 mV/dec. Note that this small SS value is close to the theoretical limit (60 mV/dec), indicating a high-quality interface between In_2O_3:PVP channel and AlO_x dielectric.[43] In addition to the smooth surface of AlO_x dielectric film, the noncorrosive property of WI channel layer is also beneficial to form a high-quality interface. The maximum areal density of states (N_s^{max}) at In_2O_3:PVP/AlO_x interface was calculated to be 7.5×10^{11} cm^{-2}. This value is smaller than that of the TFTs based on CVD-derived AlO_x (2.7×10^{12} cm^{-2}),[44] anodic Al_2O_3 (1.2×10^{12} cm^{-2}),[45] sputtered AlO_x (1.1×10^{13} cm^{-2}),[46] and organic-based spin-coated AlO_x[16] (1.1×10^{12} cm^{-2}) dielectrics. The small N_s^{max} will not only benefit to carrier transport in the interface region, but also to the operational stability, where the hysteresis shift observed is almost irrelevant

Generally, the high-k dielectrics bring about an increase in carrier mobility by an excellent heterogeneous interfacial layer.[47] However, in the recent reports based on solution-processed TFTs, the high-mobility-driven studies suffered serious problems, such as the small I_{on}/I_{off} (I_{off} >10^{-9} A) and large SS values.[6, 8, 16, 48-50] Large I_{off} decreases the I_{on}/I_{off}, which results in more power dissipation, and yields TFT unstable and unreliable. In these works, the high-k dielectrics were prepared using organic-based precursor solutions. During the post-annealing process, the pyrolysis of organic ligands tends to release a large amount of the volatile gases, which can generate nano-pores in the resultant dielectric films. This will be problematic for high-performance electronic devices. However, in this report, the organic-free WI precursor solution can effectively reduce the formation of the volatile gases. The UV-assisted thermal annealing process allows the moderate decomposition of nitrogen-related species in the thin film. Therefore, the TFT based on a high-quality dense AlO_x dielectric presents a high I_{on}/I_{off} of 2×10^7 with a low I_{off} of ~10^{-12} A.

Although TFT devices based on metal oxide/polymer hybrid channel layers have been realized in the previous works, there is still a vacancy about the discussing on TFTs' stability under bias voltage.[22, 23] For practical applications, it's crucial to exhibit voltage independent stability and reliability, especially for low-temperature processed TFT devices. To investigate the bias stability of the WI In_2O_3:PVP/AlO_x

RSC Advances Accepted Manuscript

TFT, the positive bias stress (PBS) test was carried out by applying a constant gate voltage of 2 V while maintaining source and drain electrodes grounded. Fig. 8(a) shows the transfer curves as a function of the applied stress time for 250 ^{o}C-annealed In_2O_3:PVP/AlO_x TFT. The resulting V_{TH} versus bias time is shown in Fig. 8(b). Even without passivation, the hybrid TFT exhibits high operational stability with a small threshold voltage shift (ΔV_{TH}) of 0.08 V for 5400 s. The stress induced ΔV_{TH} is in good agreement with the hysteresis shift in the double-sweep mode, which is consistent with the charge trapping mechanism at the channel/dielectric interface.[51] The parallel V_{TH} shift, without a change in the *SS* value, indicates that no additional defect states were created at the interface region under bias stressing.[4] In addition, the V_{TH} instability of bottom gate TFT devices is also related to the atmospheric oxygen and the moisture adsorption on the surface of the channel layer.[52] When PBS is applied under atmospheric conditions, O_2 adsorption is known to form a depletion layer below the channel surface, leading to a positive V_{TH} shift.[53] The chemical reaction and the proposed band diagram are shown in the inset of Fig. 8(b). A further work on the passivation or encapsulation of the TFT cannel will be effective to physically prevent ambient molecules from adsorbing on channel back surface.

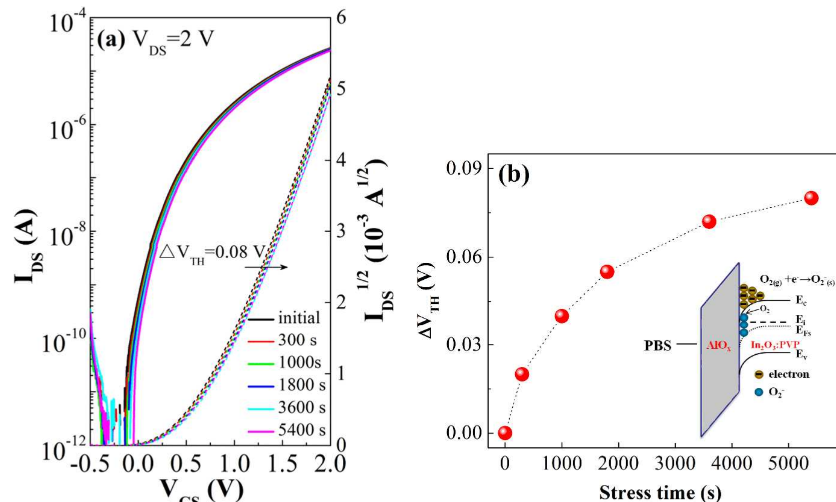

Fig. 8 (a) Transfer curves of 250 ^{o}C-annealed In_2O_3:PVP TFT under PBS with a V_G value of 2 V for 5400 s. (b) The V_{TH} shift as a function of stress time. The inset shows the energy band diagram of the In_2O_3:PVP/AlO_x TFT under PBS test.

Based on the outstanding electrical performance of the WI In_2O_3:PVP/AlO_x TFT, the eco-friendly water-inducement process can undoubtedly replace the conventional organic-based approach to achieve low-temperature, low-power consumption, and high-performance TFTs. The achievement of the WI low-operating voltage metal-oxide/polymer hybrid TFT not only opens a new route for low-temperature processed

RSC Advances Accepted Manuscript

amorphous semiconductors, but also contributes to the development of the flexible electronics.

4. Conclusion

In this report, the eco-friendly water-inducement method was introduced to fabricate the high-*k* AlO_x dielectric and the hybrid TFTs. The TGA results indicated that AlO_x dielectric formation was achieved at temperatures up to 350 ^oC, whereas conventional 2-ME-based route required far greater temperatures. The resulting WI AlO_x dielectric layer annealed at 350 ^oC was amorphous and exhibited high electrical performance, such as a low leakage current density of 0.4 nA/cm^2 at 1 MV/cm and a large flat areal-capacitance of 413 nF/cm^2 at 10 kHz. The optimized WI In_2O_3:PVP TFTs based on AlO_x, annealed at 250 ^oC, exhibit outstanding performances such as a μ_{sat} of 14.1 cm^2/Vs, a *SS* of 80 mV/dec, a I_{on}/I_{off} of 2×10^7, highly stable (a $\Delta V < 90$ mV, after bias stress, by more than 5400 s) and a low operating voltage of 2 V. This study demonstrates that the environmental friendly water-inducement method not only opens a new route for fabricating high-*k* dielectric films at low temperature, but also achieves the organic/inorganic hybrid compositions for the next-generation functional electronics.

Acknowledgements

This study was supported by Natural Science Foundation of China (Grant no. 51472130 and 51572135) and Natural Science Foundation of Shandong Province (Grant no. ZR2012FM020).

References

1 K. Nomura, H. Ohta, A. Takagi, T. Kamiya, M. Hirano, H. Hosono, *Nature* 2004, **432**, 488-492.

2 E. Fortunato, P. Barquinha, R. Martins, *Adv. Mater.* 2012, **24**, 2945-2986.

3 R. Martins, E. Fortunato, P. Barquinha, L. Pereira, *Transparent oxide electronics: from materials to devices*. John Wiley & Sons: 2012.

4 G. X. Liu, A. Liu, F. K. Shan, Y. Meng, B. C. Shin, E. Fortunato, R. Martins, *Appl. Phys. Lett.* 2014, **105**, 113509-113513.

RSC Advances Accepted Manuscript

5 K. Banger, Y. Yamashita, K. Mori, R. Peterson, T. Leedham, J. Rickard, H. Sirringhaus, *Nat. Mater.* 2010, **10**, 45-50.

6 M. G. Kim, M. G. Kanatzidis, A. Facchetti,T. J. Marks, *Nat. Mater.* 2011, **10**, 382-388.

7 Y. H. Kim, J. S Heo, T. H. Kim, S. Park, M. H. Yoon, J. Kim, M. S. Oh, G. R. Yi, Y. Y. Noh, S. K. Park, *Nature* 2012, **489**, 128-132.

8 S. Y. Cho, E. J. Bae, Y. H. Kang, M. Han, C. Lee, *J. Mater. Chem. C* 2014, 2, 5695-5703.

9 P. K. Nayak, M. Hedhili, D. Cha, H. Alshareef, *Appl. Phys. Lett.* 2013, **103**, 033518-033521.

10 L. Prabhumirashi, J. Khoje, *Thermochim. Acta* 2002, **383**, 109-118.

11 S. Jeong, J. Y. Lee, S. S. Lee, Y. Choi, B. H. Ryu, *J. Phys. Chem. C* 2011, **115**, 11773-11780.

12 A. Liu, G. X. Liu, H. H. Zhu, F. Xu, E. Fortunato, R. Martins, F. K. Shan, *ACS Appl. Mater. Interfaces* 2014, **6,** 17364-17369.

13 Y. H. Hwang, J. S. Seo, J. M. Yun, H. Park, S. Yang, S. H. Park, B. S. Bae, *NPG Asia Mater.* 2013, **5**, e45-e52.

14 G. X. Liu, A. Liu, H. H. Zhu, B. C. Shin, E. Fortunato, R. Martins, Y. Q. Wang, F. K. Shan, *Adv. Funct. Mater.* 2015, **25**, 2564-2572.

15 C. Avis, H. R. Hwang, J. Jang, *ACS Appl. Mater. Interfaces* 2014, **6**, 10941-10945.

16 W. Y. Xu, H. Wang, L. Ye, J. B. Xu, *J. Mater. Chem. C* 2014, **2**, 5389-5396.

17 R. Branquinho, D. Salgueiro, L. Santos, P. Barquinha, L. Pereira, R. Martins, E. Fortunato, *ACS Appl. Mater. Interfaces* 2014, **6**, 19592-19599.

18 J. W. Hennek, M. G. Kim, M. G. Kanatzidis, A. Facchetti, T. J. Marks, *J. Am. Chem. Soc.* 2012, **134**, 9593-9596.

RSC Advances Accepted Manuscript

19 A. Olziersky, P. Barquinha, A. Vilà, C. Magana, E. Fortunato, J. Morante, R. Martins, *Mater. Chem. Phys.* 2011, **131**, 512-518.

20 J. I. Kim, K. H. Ji, M. Jang, H. Yang, R. Choi, J. K. Jeong, *ACS Appl. Mater. Interfaces* 2011, **3**, 2522-2528.

21 J. H. Kim, Y. S. Rim, H. J. Kim, *ACS Appl. Mater. Interfaces* 2014, **6**, 4819-4822.

22 C. Kagan, D. Mitzi, C. Dimitrakopoulos, *Science* 1999, **286**, 945-947.

23 X. G. Yu, L. Zeng, N. Zhou, P. Guo, F. Shi, D. B. Buchholz, Q. Ma, J. Yu, V. P. Dravid, R. P. H. Chang, M. Bedzyk, T. J. Marks, A. Facchetti, *Adv. Mater.* 2015, **27**, 2390-2399.

24 D. K. Schroder, *Semiconductor material and device characterization*. John Wiley & Sons: 2006.

25 L. Zhang, J. Li, X. Zhang, X. Jiang, Z. Zhang, *Appl. Phys. Lett.* 2009, **95**, 072112-072114.

26 T. Schneller, R. Waser, M. Kosec, D. Payne, *Chemical Solution Deposition of* Functional *Oxide Thin Films*. Springer: 2010.

27 S. Parthiban, J. Y. Kwon, *J. Mater. Res.* 2014, **29**, 1585-1596.

28 J. Robertson, *Rep. Prog. Phys.* 2006, **69**, 327-396.

29 J. Hwang, K. Lee, Y. Jeong, Y. U. Lee, C. Pearson, M. C. Petty, H. Kim, *Adv. Mater. Interfaces* 2014, **1**, 1400206-1400214.

30 S. Goldstein, J. Rabani, *J. Am. Chem. Soc.* 2007, **129**, 10597-10601.

31 J. Mack, J. R. Bolton, *J. Photoch. Photobio A* 1999, **128**, 1-13.

32 J. Peng, Q. J. Sun, S. D. Wang, H. Q. Wang, W. L. Ma, *Appl. Phys. Lett.* 2013, **103**, 061603-061606.

33 J. T. Kloprogge, L. V. Duong, B. J. Wood, and R. L. Frost, *J. Colloid Interface Sci.* 2006, **296**, 572-576.

RSC Advances Accepted Manuscript

34 Y. B. Yoo, J. H. Park, K. H. Lee, H. W. Lee, K. M. Song, S. J. Lee, H. K. Baik, *J. Mater. Chem. C* 2013, **1**, 1651-1658.

35 J. H. Park, Y. B. Yoo, K. H. Lee, W. S. Jang, J. Y. Oh, S. S. Chae, H. W. Lee, S. W. Han, H. K. Baik, *ACS Appl. Mater. Interfaces* 2013, **5**, 8067-8075.

36 C. Avis, J. Jang, *J. Mater. Chem.* 2011, **21**, 10649-10652.

37 P. N. Plassmeyer, K. Archila, J. F. Wager, C. J. Page, *ACS Appl. Mater. Interfaces* 2015, **7**, 1678-1684.

38 K. M. Kim, C. W. Kim, J. S. Heo, J. Na, J. E. Lee, C. B. Park, J. U. Bae, C. D. Kim, M. Jun, Y. K. Hwang, S. T. Meyers, A. Grenville, D. A. Keszler, *Appl. Phys. Lett.* 2011, **99**, 242109-242111.

39 M. Zheng, M. Gu, Y. Jin, G. Jin, *Mater. Sci. Eng. B* 2000, **77**, 55-59.

40 M. Sun, G. Zou, S. Xu, X. Wang, *Mater. Chem. Phys.* 2012, **134**, 309-316.

41 J. H. Park, Y. B. Yoo, K. H. Lee, W. S. Jang, J. Y. Oh, S. S. Chae, H. K. Baik, *ACS Appl. Mater. Interfaces* 2013, **5**, 410-417.

42 S. H. Jeong, Y. G. Ha, J. H. Moon, T. J. Marks, A. Facchetti, *Adv. Mater.* 2010, **22**, 1346-1350.

43 M. Lorenz, H. von Wenckstern, M. Grundmann, *Adv. Mater.* 2011, **23**, 5383-5386.

44 M. Furuta, T. Kawaharamura, D. Wang, T. Toda, T. Hirao, *IEEE Electr. Device Lett.* 2012, **33**, 851-853.

45 L. F. Lan, J. B. Peng, *IEEE T. Electron Dev.* 2011, **58**, 1452-1455.

46 J. Li, F. Zhou, H. P. Lin, W. Q. Zhu, J. H. Zhang, X. Y. Jiang, Z. L. Zhang, *Curr. Appl. Phys.* 2012, **12**, 1288-1291.

47 Y. S. Rim, H. Chen, X. Kou, H. S. Duan, H. Zhou, M. Cai, H. J. Kim, Y. Yang, *Adv. Mater.* 2014, **26**, 4273-4278.

48 G. Adamopoulos, S. Thomas, D. D. Bradley, M. A. McLachlan, T. D.

RSC Advances Accepted Manuscript

Anthopoulos, *Appl. Phys. Lett.* 2011, **98**, 123503-123505.

49 W. Yang, K. Song, Y. Jung, S. Jeong, J. Moon, *J. Mater. Chem. C* 2013, **1**, 4275-4282.

50 J. H. Park, K. Kim, Y. B. Yoo, S. Y. Park, K. H. Lim, K. H. Lee, H. K. Baik, Y. S. Kim, *J. Mater. Chem. C* 2013, **1**, 7166-7174.

51 R. Branquinho, D. Salgueiro, A. Santa, A. Kiazadeh, P. Barquinha, L. Pereira, R. Martins, E. Fortunato, *Semicond. Sci. Tech.* 2015, **30**, 024007-024014.

52 J. K. Jeong, H. W. Yang, J. H. Jeong, Y. G. Mo, H. D. Kim, *Appl. Phys. Lett.* 2008, **93**, 123508-123510.

53 J. W. Hennek, J. Smith, A. Yan, M. G. Kim, W. Zhao, V. P. Dravid, A. Facchetti, T. J. Marks, *J. Am. Chem. Soc.* 2013, **135**, 10729-10741.

RSC Advances Accepted Manuscript